A&A 447, 49–62 (2006)
DOI: 10.1051/0004-6361:20053210

Astronomy & Astrophysics

H I study of the warped spiral galaxy NGC 5055: a disk/dark matter halo offset?

G. Battaglia[1], F. Fraternali[2], T. Oosterloo[3], and R. Sancisi[4]

[1] Kapteyn Astronomical Institute, Postbus 800, 9700 AV, Groningen, The Netherlands
e-mail: gbattagl@astro.rug.nl
[2] Theoretical Physics, University of Oxford, 1 Keble Road, OX1 3NP, Oxford, UK
[3] ASTRON, Postbus 2, 7990 AA, Dwingeloo, The Netherlands
[4] INAF – Osservatorio Astronomico, via Ranzani 1, 40127, Bologna, Italy and Kapteyn Astronomical Institute, University of Groningen, PO Box 800, The Netherlands

Received 7 April 2005 / Accepted 8 September 2005

ABSTRACT

We present a study of the H I distribution and dynamics of the nearby spiral galaxy NGC 5055 based on observations with the Westerbork Synthesis Radio Telescope. The gaseous disk of NGC 5055 extends out to about 40 kpc, equal to 3.5 R_{25}, and shows a pronounced warp that starts at the end of the bright optical disk (R_{25} = 11.6 kpc). This very extended warp has large-scale symmetry, which along with the rotation period of its outer parts (≃1.5 Gyr at 40 kpc), suggests a long-lived phenomenon.

The rotation curve rises steeply in the central parts up to the maximum velocity ($v_{\rm max} \simeq 206$ km s^{-1}). Beyond the bright stellar disk (R_{25}), it shows a decline of about 25 km s^{-1} and then remains flat out to the last measured point. The standard analysis with luminous and dark matter components shows the dynamical importance of the disk. The best fit to the rotation curve is obtained with a "maximum disk". Less satisfactory fits with lighter disks help to set a firm lower limit of 1.4 to the mass-to-light ratio in F band of the disk. Such a "minimum disk" contributes about 60% of the observed maximum rotational velocity.

NGC 5055 shows remarkable overall regularity and symmetry. A mild lopsidedness is noticeable, however, both in the distribution and kinematics of the gas. The tilted ring analysis of the velocity field led us to adopt different values for the kinematical centre and for the systemic velocity for the inner and the outer parts of the system. This has produced a remarkable result: the kinematical and geometrical asymmetries disappear, both at the same time. These results point at two different dynamical regimes: an inner region dominated by the stellar disk and an outer one, dominated by a dark matter halo offset with respect to the disk.

Key words. galaxies: individual: NGC 5055 – galaxies: kinematics and dynamics – galaxies: structure – galaxies: ISM – cosmology: dark matter

1. Introduction

NGC 5055 is an Sbc spiral galaxy (de Vaucouleurs et al. 1976) at a distance of 7.2 Mpc (Pierce 1994). At this distance 1′ ≃ 2.1 kpc. Figure 1 (top left) shows the DSS image. The main optical and radio parameters are listed in Table 1.

Previous 21-cm line observations (Bosma 1978) have shown the presence of an extended, warped gaseous disk and a declining rotation curve. In this study we used new Westerbork Synthesis Radio Telescope (WSRT) observations to study the warp and the dynamics of the system.

The warp starts at the end of the bright stellar disk, around R_{25}, and is exceptionally extended and symmetric. This suggests a stable dynamics that precludes recent formation. Warps are still poorly understood phenomena. They are very common and ubiquitous (e.g. Garcia-Ruiz et al. 2002, and references therein), but it is not clear yet whether this means that they are easily excited or that there is a mechanism capable of maintaining them. Several different possibilities have been proposed to explain their origin such as: tidal interactions (Burke 1957; Kerr 1957; Hunter & Toomre 1969), misalignment between disk and halo (Debattista & Sellwood 1999), discrete bending modes due to a tilted oblate dark matter halo (Sparke & Casertano 1988), effects of the intergalactic medium and accretion (Kahn & Woltjer 1959; Jiang & Binney 1999). In particular, the possible role of dark matter halos has been widely considered. However, none of these explanations has been completely accepted.

The rotation curve of NGC 5055 shows a decline at the end of the bright optical disk. Both rotation curves with a similar shape and correlations with the luminosity and light distribution have been known to exist (Casertano & van Gorkom 1991; Persic & Salucci 1991; Broeils 1992). They seem to point at rules in the distribution and relative dynamical contributions of the luminous and dark components. In particular, velocity

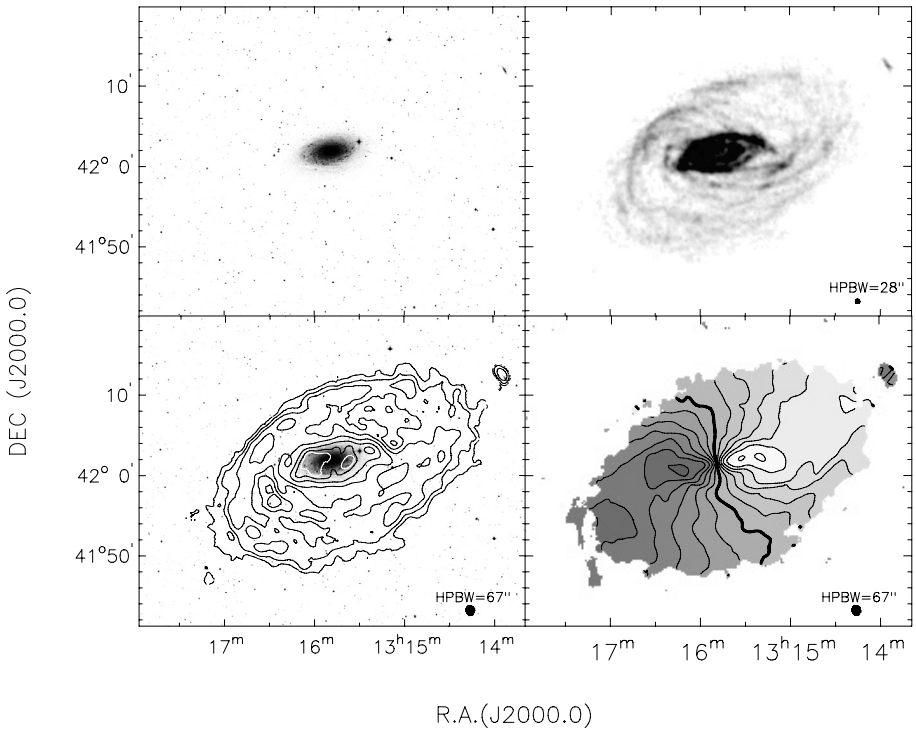

Fig. 1. *Top left*: optical image (DSS) of NGC 5055. *Top right*: total H I map at 28″ resolution. *Bottom left*: total H I map at 67″ resolution overlaid with the DSS optical image; contours are 3.0, 6.0, 12.0, 20.6, 41.2, 82.4, 123.4 × 10^{19} cm^{-2}. *Bottom right*: velocity field at 67″ resolution; contours are separated by 30 km s^{-1}, and the thick line shows the systemic velocity (497.6 km s^{-1}); the receding side is S–E.

Table 1. Optical and Radio Parameters for NGC 5055. (1) De Vaucouleur et al. (1976); (2) Maoz et al. (1996); (3) this work; (4) Pierce (1994); (5) Kent (1987), using a distance of 7.2 Mpc; (6) Holmberg (1958). $M_*(<R_{\rm out})$ and $M_{\rm DM}(<R_{\rm out})$ are, respectively, the mass of the stellar disk and of the dark matter halo within the last measured point (≃40 kpc), derived in the maximum disk hypothesis with isothermal halo.

Parameter	NGC 5055	Ref.
Morphological type	SA(rs)bc II	1
Optical centre (α, δ J2000)	$13^{\rm h}15^{\rm m}49.25^{\rm s}$ +42°01′49.3″	2
Kinematical centre (α, δ J2000)	$13^{\rm h}15^{\rm m}49.2^{\rm s}$ +42°01′49.0″	3
Distance (Mpc)	7.2	4
L_B ($L_{\odot B}$)	2.55×10^{10}	1
Disk scale length (′)	1.6	5
R_{25} (′)	5.5	1
Holmberg diametres (′)	16 × 10	6
Systemic velocity (km s^{-1})	497.6 ± 4.8	3
$M_{\rm HI}$	$6.2 \pm 0.3 \times 10^9$ $M_\odot$	3
$M_*(<R_{\rm out})$	8×10^{10} $M_\odot$	3
$M_{\rm DM}(<R_{\rm out})$	1.9×10^{11} $M_\odot$	3

declines may be indications of a dominant contribution of the stellar disk in the inner parts and of a transition to a dark halo in the outer parts.

NGC 5055 also shows the presence of gas rotating with velocities lower than the rotational velocities of the disk. Such "anomalous" gas has already been detected in several other spiral galaxies seen at various inclination angles (e.g. Fraternali et al. 2002; Boomsma et al. 2005) and has been interpreted as gas residing in their halo regions (Swaters et al. 1997).

Table 2. Observational parameters for NGC 5055.

Parameter	NGC 5055
Observation dates	22-04-2001, 11-05-2001
Length of observation	12 h each
Number of antennas	14
Baseline (min-max-incr)	36-m 2700-m 36-m
Pointing RA (J2000)	$13^{\rm h}15^{\rm m}49.20^{\rm s}$
Pointing Dec (J2000)	42°01′48.99″
Frequency of observation (MHz)	1420.406
Total bandwidth (MHz)	5
Total bandwidth (km s^{-1})	948
Number of channels	128
Central velocity (km s^{-1})	540
Channel separation (kHz)	38.7
Channel separation (km s^{-1})	8.24
Spectral resolution (km s^{-1})	16.48

The new high sensitivity and high resolution H I observations of NGC 5055 with the WSRT allow us to investigate all the aspects mentioned above.

2. Observations and data analysis

We observed NGC 5055 with the DZB spectrometer of the Westerbork Synthesis Radio Telescope. The WSRT observing parameters are given in Table 2. Calibration and data reduction were done using standard procedures of the MIRIAD (Multichannel Image Reconstruction, Image Analysis and Display) package (Sault et al. 1995). Twenty-two channels free of line emission were identified at the low velocity end of the

Table 3. Parameters of the Data Cubes used.

Parameter	18″	28″	67″
HPBW (″)	23.5×13.9	31.6×25.0	74.7×59.3
PA of synthesized beam (°)	1.3	11.2	10.1
Beam size (kpc)	0.82×0.49	1.10×0.87	2.61×2.07
rms noise per channel (mJy/beam)	0.3	0.4	0.6
rms noise per channel (K)	0.6	0.3	0.1
Minimum detectable column density:			
per resolution element (cm^{-2})	8.4×10^{19}	4.6×10^{19}	1.2×10^{19}
per resolution element ($M_\odot/pc^2$)	0.67	0.37	0.10
Conversion factor (K/mJy)	2.0	0.75	0.17

band and twenty-four at the high velocity end. The radio continuum emission was obtained by interpolating with a straight line and then subtracted from the line channels. Three data cubes at different angular resolutions were obtained. The full resolution (18″ ≃ 627 pc) data cube was obtained using all baselines. For the data cubes at resolutions of 28″ and 67″, we used baselines shorter than 5kλ and 3kλ, respectively. Table 3 lists the parameters for the data cubes. A Hanning smoothing was then applied in velocity leading to a resolution of 16 km s^{-1}. The dirty channel maps were cleaned using a Clark CLEAN algorithm (Clark 1980). The final data cubes (at 18″, 28″, 67″ resolution) have rms noises per channel of 0.3, 0.4, 0.6 mJy/beam respectively. In these cubes the respective minimum detectable column densities in one velocity resolution element (at 5σ) are 8.4×10^{19} cm^{-2} (0.67 $M_\odot$/pc^2), 4.6×10^{19} cm^{-2} (0.37 $M_\odot$/pc^2), and 1.2×10^{19} cm^{-2} (0.10 $M_\odot$/pc^2).

Comparison between the global H I profile from these observations and from single dish measurements (Rots 1980) shows that there is no loss of H I flux due to the missing short spacings (Fig. 2).

The cleaned data cubes were analyzed using the Groningen Image Processing System (GIPSY) package (van der Hulst et al. 1992). Channel maps at 67″ resolution, with a separation of 27 km s^{-1} and without primary beam correction, are shown in Fig. 3. These channel maps show the well-known pattern of a differentially rotating disk and a very extended warp in the outer parts.

2.1. Total H I maps and velocity fields

For each resolution (18″, 28″, 67″), total H I maps were obtained by adding the channel maps containing neutral hydrogen emission (from ≃280 km s^{-1} to ≃730 km s^{-1}). The area containing line emission was defined by visual inspection. The total H I mass, corrected for the primary beam attenuation, is $6.2 \pm 0.3 \times 10^9$ $M_\odot$. The value obtained by Bosma (1978) is 6.3×10^9 $M_\odot$, after correction for the distance adopted in this work. For comparison, the single-dish mass (Rots 1980) is 5.9×10^9 $M_\odot$.

Figure 1 shows the total H I map at 28″ resolution (top right) and at 67″ resolution overlaid with the DSS optical image (bottom left). The H I disk extends out to about 3.5 R_{25} (see Table 1), equal to 40 kpc. The extent derived from previous observations of lower sensitivity (Bosma 1978) was 37 kpc. The high surface brightness part of the H I disk (dark gray in Fig. 1) has the same extent (about 10 kpc) and orientation as the bright optical disk. The outer parts show a change in orientation of about 20° as compared to the inner region due to the warping of the H I disk (see Sect. 4).

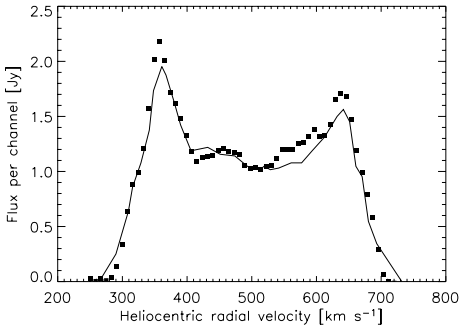

Fig. 2. Comparison between the global H I profile of NGC 5055 from this work (squares) and from single dish observations (full line) by Rots (1980).

Remarkably, the extended, warped HI layer shows spiral arm features and a large-scale pattern (arms or ring) in the density distribution. In the velocity field there are wiggles possibly associated with these spiral arms that suggest the presence of streaming motions.

Velocity fields for each of the three resolutions were obtained by fitting Gaussians to the velocity profiles. This method gives good results except in the very central region ($R \leq 18'' = 627$ pc), where the velocity profiles are affected by beam smearing. Figure 1 (bottom right) shows the radial velocity field at low resolution (67″). This velocity field is very symmetric and, in the outer parts, shows the characteristic behaviour of a kinematical warp: the position angle of the kinematical major axis varies with the radius, from a value of about 100° within $R_{\rm Ho}$ to about 120° in the outer region. Wiggles are visible especially in the S-W side.

2.2. UGC 8313

We also detected neutral hydrogen emission from a companion galaxy of NGC 5055, UGC 8313, a small galaxy of type SBc (Tully 1988) at $\alpha = 13^{\rm h}13^{\rm m}54.1^{\rm s}$, $\delta = 42°12'35.7''$ (2MASS, 2000), at a projected distance of 50 kpc to the North-West

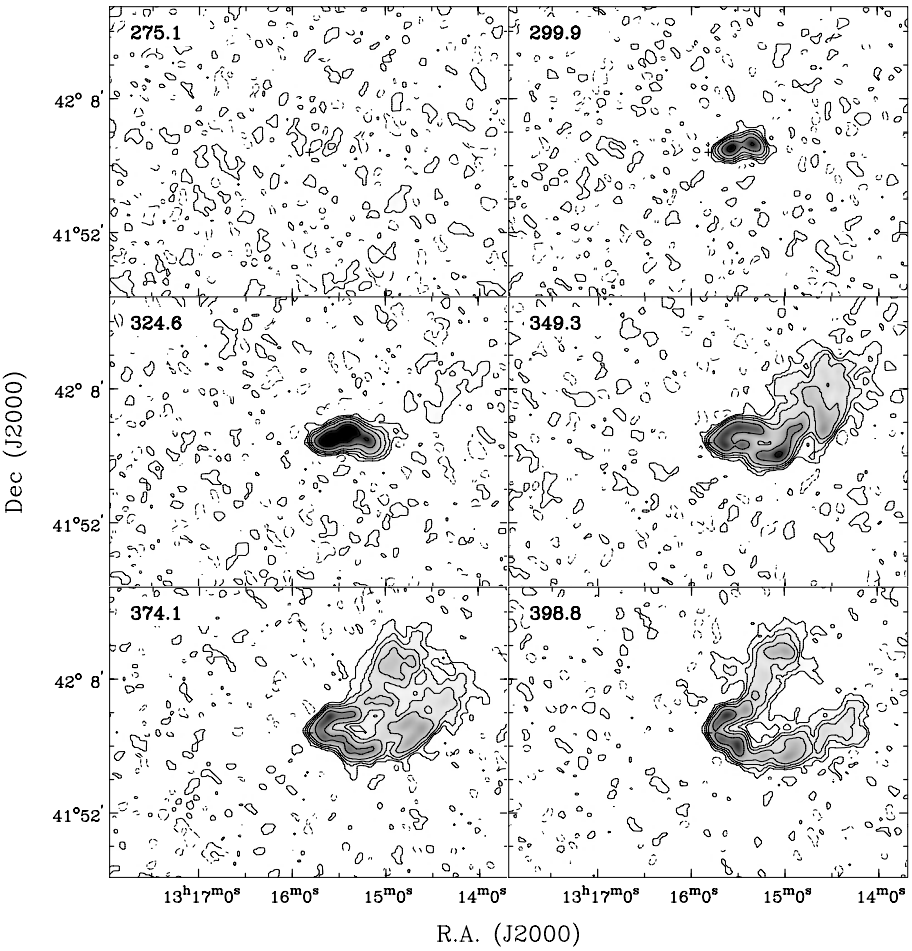

Fig. 3. H I channel maps of NGC 5055 at 67″ resolution (Hanning smoothed). Contours are −1.2 (dashed), 1.2, 3, 6, 12, 30, 60, 120, 300 mJy/beam; the rms noise is 0.6 mJy/beam. The heliocentric velocities (in km s^{-1}) are shown in the upper left corner; the cross indicates the kinematical centre of the galaxy.

of NGC 5055 (Fig. 1 and channel maps from 571.9 km s^{-1} to 670.9 km s^{-1}, Fig. 3). By integrating the H I channel maps at 18″ resolution from ≃555 km s^{-1} to ≃687 km s^{-1}, we obtained a total H I mass, corrected for the primary beam attenuation, of $7\times10^7\ M_\odot$. In comparison, Bosma (1978) found a total H I mass of $2.8\times10^7\ M_\odot$ (with a distance of 7.2 Mpc). From the global H I profile, we obtained a systemic velocity, $v_{\rm sys} \simeq 620$ km s^{-1}. The spatial resolution of our data was too low and the object too small ($R \simeq 1' \simeq 2.1$ kpc) to derive a detailed rotation curve. But taking the effects of bandwidth and the uncertain inclination angle (the galaxy seems almost edge-on) into account, we set a firm lower limit for the rotational velocity, $v_{\rm max} \geq 50$ km s^{-1}. This value was derived both from the global H I profile and from the position-velocity diagram along the major axis. We estimated the total mass of UGC 8313 to be $M = 1.2\times10^9\ M_\odot$, which represents a lower limit because we do not observe the flat part of the rotation curve and we do not know the exact extent of the disk.

3. Determination of the rotation curve

In order to obtain the kinematical parameters and the rotation curve for NGC 5055, a tilted ring model (Begeman 1987) was fitted to the observed velocity fields at different resolutions. The tilted ring model assumes that a spiral galaxy can be described by a set of concentric rings. Each ring is characterized by two orientation angles (position angle ϕ and inclination angle i) and the circular velocity $v_{\rm C}$. Every ring is assumed to have the same value for the dynamical centre and the systemic velocity. At each resolution, the rings were fitted with a radial increment of the corresponding beam-width. The points were weighted by the cosine of the azimuthal angle with respect to the major axis.

An iterative procedure was followed. To determine the dynamical centre, only the points within 11.6 kpc (corresponding to R_{25}) in the velocity field at full resolution were used. While keeping this position of the centre fixed, the systemic velocity was fitted. Figure 5 shows that the systemic velocity is not constant. The average value within 230″ (≃8 kpc) is ≃492 km s^{-1}, while in the outer parts it is ≃500 km s^{-1}. This may suggest a dynamical decoupling of the central part with respect to the outer part of the galaxy (see Sect. 5). The mean systemic velocity (line in Fig. 5) was estimated as the weighted mean of the points at full resolution within the bright optical disk (11.6 kpc). Points within 60″ (≃2 kpc) were excluded in the fitting procedure because of beam-smearing and insufficient

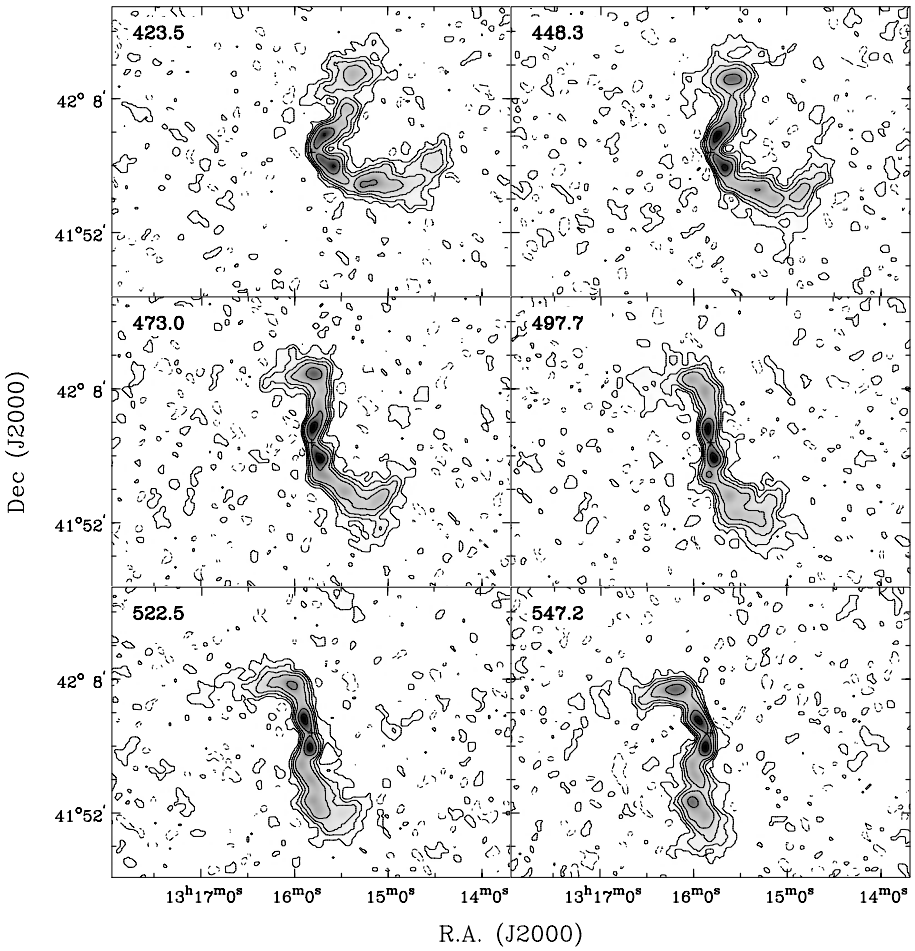

Fig. 3. continued.

statistics. The values found for the kinematical centre and for the systemic velocity are reported in Table 1.

We held the above parameters (centre and systemic velocity) fixed and we fitted first the position angle and then the inclination angle. The full-resolution data were used for the region within ≃400″ (14 kpc), and for larger distances we used the data at lower resolution. The position angle has a constant value (≃100°) in the inner part; between R_{25} (11.6 kpc) and $R_{\rm Ho}$ (16.7 kpc) it decreases by 10° and further out rises to 120° at the last measured point (Fig. 5, top right). The trend found by Bosma (1978) is very similar: he gives an average value of 99° for the inner part and 115° for the outer part. The inclination angle shows an almost constant value of 64° out to R_{25}. Beyond that region it decreases to 50° and then increases in the outer parts (mean value ≃55°). Because of the large errors in the fit of the inner part, the value of the inclination angle was fixed to 63° within 30″ (1 kpc). Bosma assumed a constant value of 55° for the whole galaxy; Pierce et al. (1994), with photometric CCD observations, found 64° for the inner part.

Finally, after having determined all the above parameters, we derived the circular velocity. The rotation curve (Fig. 5, bottom right) reaches the maximum velocity, $v_{\rm max}$ = 206 km s^{-1} between 1.9 h and 2.7 h (h = 3.4 kpc). Between 10 and 20 kpc, it decreases by about 25 km s^{-1} and then becomes almost constant out to the last measured point ($R_{\rm out}$ = 19′ ≃ 40 kpc). The mass of NGC 5055 within 40 kpc derived from the circular velocity at that radius is $M(<R_{\rm out}) \simeq 2.7 \times 10^{11}\ M_{\odot}$. The error bars show the differences in circular velocities between approaching and receding side and include, therefore, the effect of deviations from circular motions. The solid line shows the rotation curve derived by Bosma (1978). In the inner regions (inside 5 kpc), the circular velocities obtained in this work are larger than the rotation velocities derived by Bosma (maximum difference 40 km s^{-1}). This difference can be explained with the lower resolution of Bosma's data (≃60″) and the consequent beam-smearing effects. Bosma obtained a maximum velocity of 214 km s^{-1}; this larger value is explained by the different inclination used to de-project the observed radial velocity ($i_{\rm Bosma}$ = 55°, $i_{\rm our}$ = 63°). The quality of the derived rotation curve can be tested by overlaying it on the data. Figure 4 (left) shows a position-velocity diagram taken at the positions of the highest projected velocities (actual major axis) as shown in the right panel of Fig. 4. From this $p - v$ diagram it is clear that the derived rotation curve follows the peak of the line profiles over the whole galaxy closely.

4. Warp

The channel maps and the velocity field of NGC 5055 show the characteristic pattern of a kinematical warp. In both the

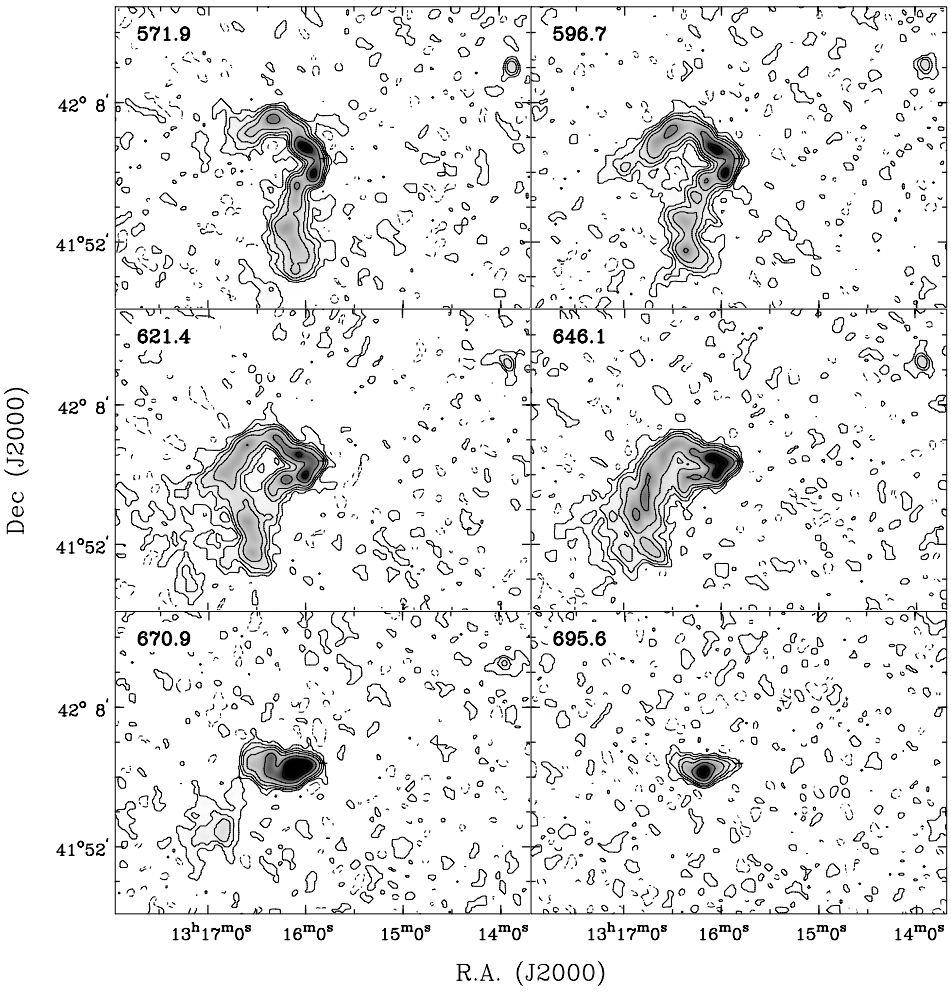

Fig. 3. continued.

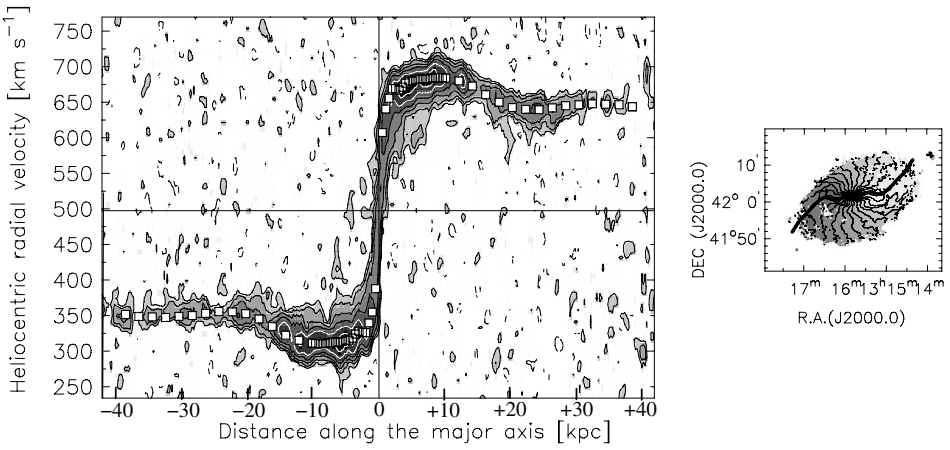

Fig. 4. *Left*: position-velocity diagram along the path (major axis) shown on the velocity field at 28″ resolution on the right (black thick line). The spatial resolution is 28″, and the velocity resolution is ∼16 km s^{-1}. Contours are −2, 2, 4, 8, 16, 32, 64, 128, 256σ, where σ = 0.4 mJy/beam. The horizontal line shows the systemic velocity. The white squares show the projected circular velocity.

H I map and the velocity field (Fig. 1), the orientation of the major axis changes with distance from the centre, varying from 100° within R_{25} to 120° in the outer region.

In order to investigate the geometry of the disk and the symmetry of the warp, the two orientation angles (position and inclination angle) were determined for the approaching and the receding sides separately (Fig. 6). The position angles of the two halves of the galaxy (Fig. 6, second panel) are similar: the only difference is in the outer region, where the receding side has values that are 15° higher than the approaching side. The behaviour of the inclination angle is similar for the two sides (Fig. 6, first panel) within 400″ (≃14 kpc). Between

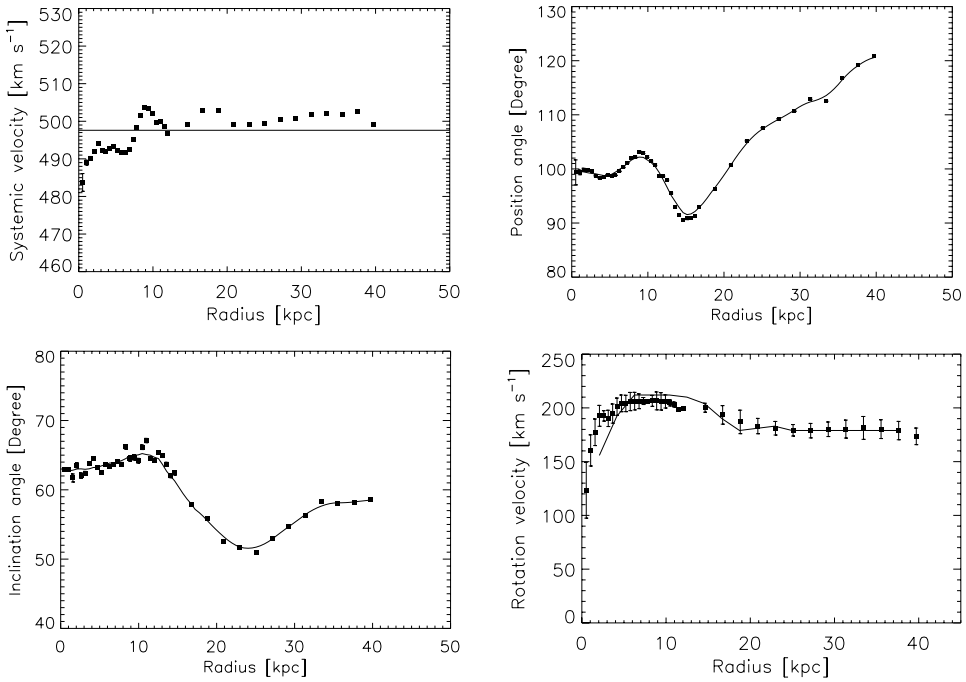

Fig. 5. Parameters for NGC 5055 obtained from the tilted ring model fit. In the *top left panel* the horizontal line shows the mean systemic velocity adopted in this work, $v_{\rm sys}$ = 497.6 km s^{-1}. The full lines in the plots for the position and inclination angles were obtained smoothing the data, in order to remove small-scale fluctuations. *Bottom right panel*: rotation curve from this work (filled squares) compared with the rotation curve (line) derived by Bosma (1978).

14 kpc and 28 kpc there are large differences, since on the approaching side, the inclination angle is almost constant around 57°, whilst on the receding part it decreases from 60° to 47 °.

These orientation angles are set with respect to the plane of the "sky". In order to display the space orientation of the rings, we used a reference frame defined by the plane of the inner galaxy (within R_{25}). We determined the angle between the plane of every ring and the plane of the inner disk, θ, as well as the angle between the line of nodes and the line of intersection of the inner disk with the plane of the "sky", β (Schwarz 1985). The trend of the θ angle shows that the inclination of the rings is almost constant within the stellar disk ($R \lesssim 10$ kpc), and then it increases monotonically with distance from the centre; the outermost ring has an inclination of 20° with respect to the central plane. There is an evident systematic difference between the two sides. The behaviour of the β angle suggests that the line of nodes changes direction monotonically with radius.

5. Symmetry of the rotation curve

In Sect. 3 we derived the rotation curve for the whole galaxy (Fig. 5). Here we investigate the symmetry of the curve by analyzing the approaching and the receding side separately. For this we have used the geometrical parameters for the approaching and the receding side as derived in the previous section. Figure 7 shows that the two halves of the galaxy have similar trends of the circular velocity, and the two curves have the same overall shape as the rotation curve derived for the whole galaxy. They show, however, a systematic difference with the rotational velocity higher on the approaching side within $R \sim 8$ kpc and lower beyond that radius. The differences are typically 15 to 20 km s^{-1}. The radius R = 8 kpc seems to represent a turnover point for the dynamical behaviour of the two halves of the galaxy. As described in Sect. 3, we also noticed that at about the same distance from the centre a sudden change of the systemic velocity occurs (see Fig. 5, top left); the value in the inner part is about 492 km s^{-1}, but beyond R = 8 kpc it becomes $v_{\rm sys} \sim 500$ km s^{-1}. This suggests that the kinematics of NGC 5055 could be better described by taking two different values for the systemic velocity: a lower value in the inner part and a higher one in the outer region. This may also imply different values for the centre of the inner and outer rings.

In the classic approach to deriving of a rotation curve with a tilted ring fit, the centre and the systemic velocity of the galaxy are kept fixed while deriving the other parameters (inclination angle, position angle, and rotation velocity). In view of the peculiar behaviour of the systemic velocity (Fig. 5, upper panel) and of the rotation curves of the approaching and receding sides (Fig. 7), we attempted to relax this procedure and to let the position of the centre and the systemic velocity vary. We first fitted the observed velocity field, allowing the kinematical centre to be free and fixing the systemic velocity at 492 km s^{-1} within 8 kpc (~230″ radius) and at 500 km s^{-1} beyond that. We found that the x position of the centre changes considerably from the inner to the outer rings, whilst the y coordinate does not show any significant variation. For simplicity, we took three constant values for the x position. Figure 8 shows the values of the coordinates we adopted and the respective intervals. Then we repeated the fitting procedure keeping these two values for the systemic velocity and the three values for the centre as fixed.

Figures 9 and 10 show the geometrical parameters and the rotation curves obtained with this procedure. The symmetry

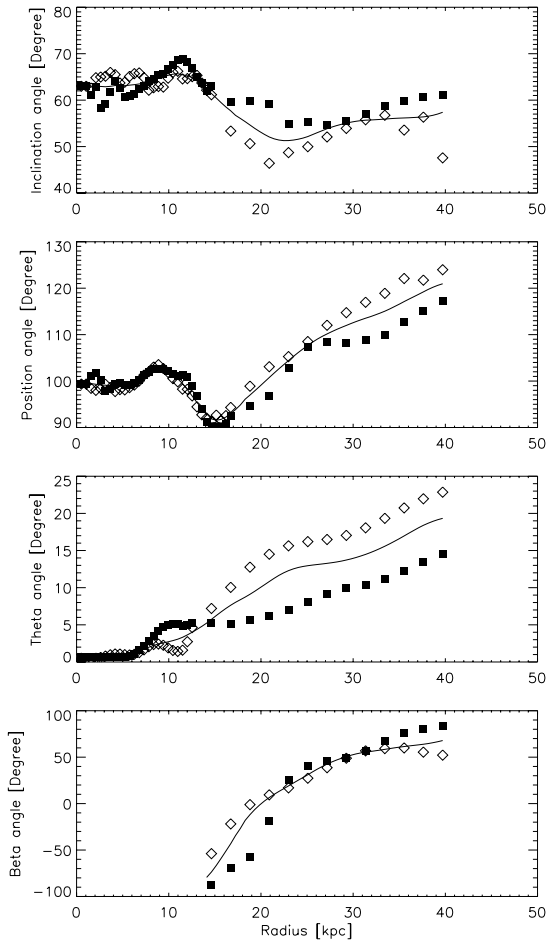

Fig. 6. Radial profiles of the geometrical parameters of the warp of NGC 5055. Filled squares show the approaching side, open diamonds the receding side, and the full line shows the parameters for the whole galaxy.

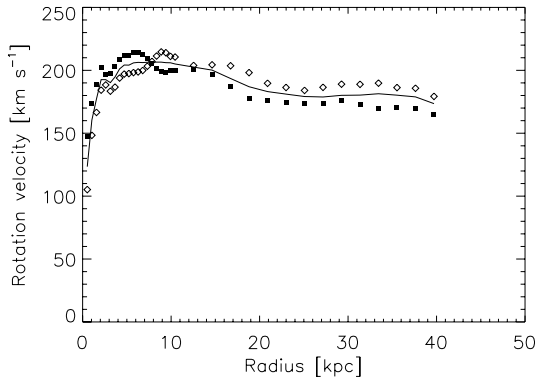

Fig. 7. Comparison between the rotation curves for NGC 5055 derived for the approaching side (filled squares) and for the receding side (open diamonds). The full line shows the rotation curve for the whole galaxy.

between the two halves of NGC 5055 is now striking, and the differences visible in Figs. 6 and 7 have disappeared. The rotation curve for the whole galaxy does not show any significant difference from the rotation curve obtained with fixed kinematical centre and systemic velocity, but the rotation curves for the approaching and receding sides now overlap almost

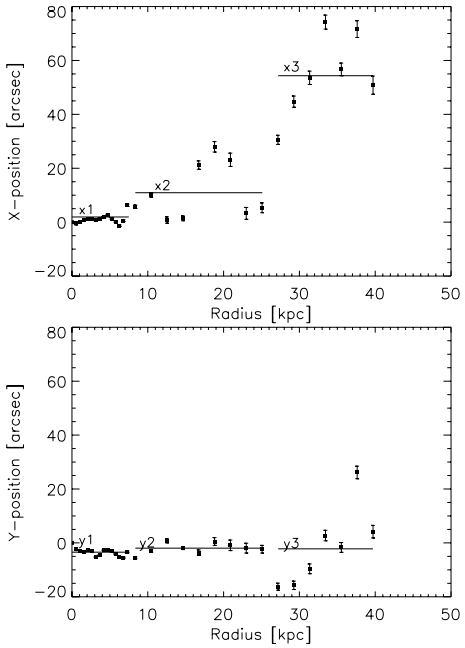

Fig. 8. Radial trend of the x (*top*) and y (*bottom*) position of the dynamical centre for NGC 5055. The horizontal lines indicate the three different values for the coordinates used in the tilted ring model fit described in Sect. 5.

completely. A discussion of these results is given in Sect. 8.3. Figure 11 shows the tilted ring model for NGC 5055 obtained with the parameters of the new fit.

It is interesting to note that similar variations of the systemic velocity have also been found in NGC 628 (Kamphuis & Briggs 1992) and in M 101 (Kamphuis 1993).

6. Mass models

The rotation curve of NGC 5055 (Fig. 10) was derived with the tilted ring model fit described in Sect. 3. Here it is used for the study of the mass distribution in NGC 5055. We consider a mass model with three components – the stellar disk, the gaseous disk, and the dark matter halo – and derive the velocity contributions that best represent the observed rotation curve through a least-square fit using a GIPSY routine. For estimating the stellar disk contribution, we used two different sets of photometric data in the "F" band.

For radii less than 7.2′ (≃15 kpc), we took the CCD brightness profile published by Kent (1987), and photographic data out to 10.3′ (≃21.5 kpc) were available from Wevers (1984). In order to match the two data sets, we added 0.2 mag/arcsec^2 to Wevers' data. Such a correction is normal when comparing photographic and CCD data (Kent 1987). To take the presence of the warp into consideration, we deprojected the brightness profile by using the inclination derived in Sect. 3. Figure 12 (top) shows the deprojected brightness profile.

The radial H I profile, shown in Fig. 13, was derived from the observed surface density (total H I map) using the parameters from the tilted ring fit. The profile shows a density drop-off in the region between 10 and 15 kpc (around R_{25}) at the location where the warp starts. For estimating the contribution of the

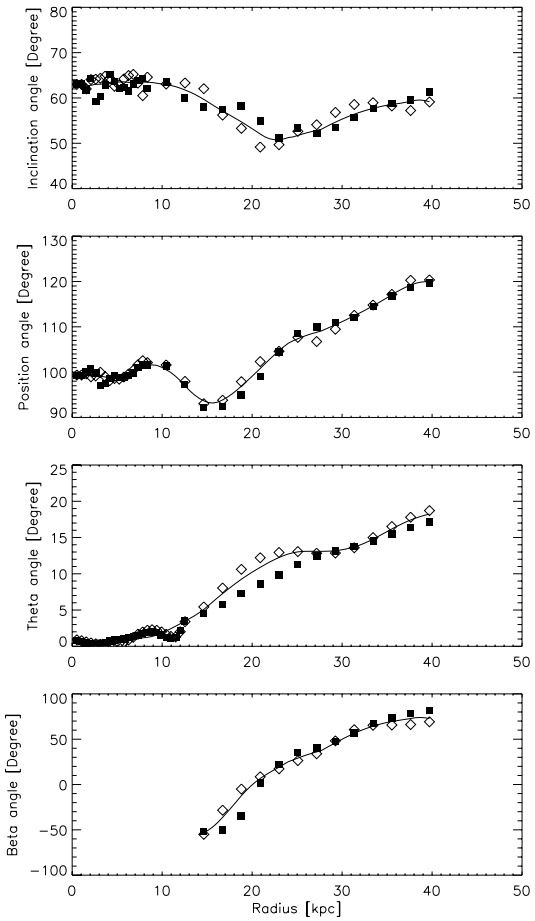

Fig. 9. Radial profiles of the warp parameters for NGC 5055, obtained using three values for the kinematical centre and two values for the systemic velocity (see Sect. 5). Filled squares show the approaching side, open diamonds the receding side, and the full line shows the parameters for the whole galaxy. Note the remarkable symmetry of the galaxy if compared with the same plots in Fig. 6.

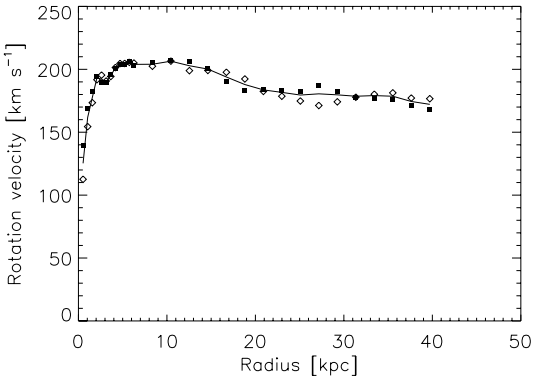

Fig. 10. Comparison between the rotation curve for the approaching side (filled squares) and receding side (open diamonds). The full line shows the rotation velocities obtained for the whole galaxy. We obtained these rotation curves using three values for the kinematical centre and two values for the systemic velocity (see Sect. 5). The two rotation curves are remarkably symmetric (compare with Fig. 7).

Fig. 11. Tilted ring model for NGC 5055 obtained from the parameters shown in Figs. 8 and 9.

gaseous disk to the rotation curve, the H I surface density was multiplied by a factor of 1.4, to take the helium abundance into account. We adopted a scale height of 0.2 kpc for the gaseous disk and 0.4 kpc for the stellar disk. The velocity contribution of the stellar component was calculated from the formula published by Casertano (1983). The available optical photometry extends out to 10.3′ (≃21.5 kpc), while the last measured point for our H I data is at 19′ (≃40 kpc). The contribution of the stellar component was calculated in the hypothesis of both an exponential disk and a drop in the brightness profile beyond 10.3′. No significant differences were found between the two cases. As usually done, the M/L ratio for the stellar component was assumed to be independent of radius.

Figure 12 (bottom) shows the contribution of the stellar component to the observed rotation velocity obtained by maximizing the stellar disk contribution in order to match the observed rotation curve in the inner parts (maximum disk hypothesis). It is clear from the large discrepancy between observed and predicted curves that a dark matter component is needed starting from well inside R_{25} to account for the observed rotational velocities.

As mass models for the dark matter halo, we adopted isothermal and NFW density profiles, as described in the following subsections.

6.1. Dark matter halo: isothermal profile

First we modeled the dark matter halo with a quasi-isothermal density profile:

$$\rho(r) = \rho_0 \left[1 + \left(\frac{r}{r_C}\right)^2\right]^{-1}$$

where ρ_0 is the central density and r_C is the core radius. The circular velocity due to this mass distribution is

$$V_c{}^2(r) = V_c{}^2(\infty)\left(1 - \frac{r_c}{r}\mathrm{arctg}\frac{r}{r_c}\right)$$

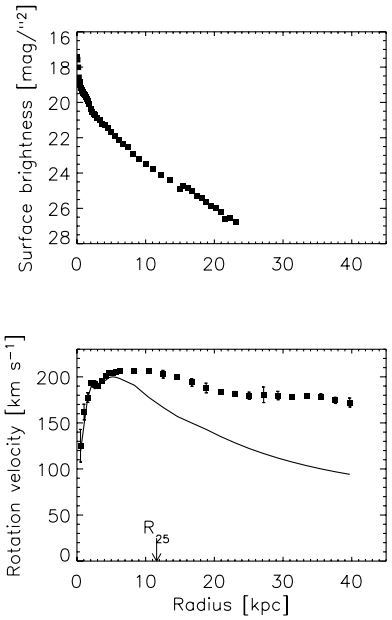

Fig. 12. *Top*: optical surface brightness profile (F band) for NGC 5055. Data within 15 kpc from the centre are from CCD observations (Kent 1987); the data in the outer parts are from photographic plates (Wevers 1984). *Bottom panel*: observed H I rotation curve (filled squares with error bars) and rotation curve calculated from the optical surface brightness profile (line).

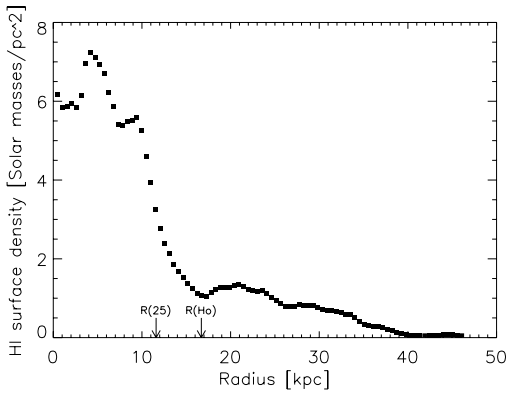

Fig. 13. Radial H I profile for NGC 5055. The arrows show the De Vaucouleurs (R_{25}) and Holmberg radii ($R_{\rm Ho}$).

where $V_{\rm c}{}^2(\infty) = 4\pi G\rho_0 r_{\rm c}^2$ is the asymptotic rotational velocity. The parameters that best fit the data are $\rho_0 = 7.6 \pm 1.9 \times 10^{-3}$ $M_\odot$ pc^{-3}, $r_{\rm c} = 8.4 \pm 1.4$ kpc, and $M/L = 3.8 \pm 0.1$ in F band, corresponding to a M/L in B band of about 3.2[1]. The above corresponds to a maximum disk fit, and gives a mass for the disk component within the last measured point $M_*(<R_{\rm out}) = 8 \times 10^{10}$ $M_\odot$, and for the dark matter halo $M_{\rm DM}(<R_{\rm out}) = 1.9 \times 10^{11}$ $M_\odot$.

This fit (Fig. 14, top left) reproduces the observed circular velocities in detail out to the region of the maximum velocity and, in particular, the feature at 2 kpc radius. The decline at the end of the bright optical disk is also reproduced. In the outer region, there is a good agreement between observed and predicted curves.

The top right panel in Fig. 14 shows the fit in the minimum disk hypothesis (the contribution of the dark matter halo is maximized), where $\rho_0 = 6.2 \pm 1.0$ $M_\odot$ pc^{-3} and $r_{\rm c} = 0.30 \pm 0.03$ kpc. For an acceptable fit, it is not possible to decrease the contribution of the disk further. This sets a firm lower limit to the stellar mass-to-light ratio: $M/L \gtrsim 1.4$. With such a value for the M/L ratio, the luminous matter is responsible for about 60% of the observed circular velocity at the peak of the rotation curve. For such a fit, $M_*(<R_{\rm out}) = 3 \times 10^{10}$ $M_\odot$ and $M_{\rm DM}(<R_{\rm out}) = 2.5 \times 10^{11}$ $M_\odot$.

6.2. Dark matter halo: NFW density profile

For the dark matter halo, we also used the universal density profile derived by Navarro et al. (1995, 1996)

$$\rho(r) = \frac{\delta_{\rm c}\rho_{\rm c}^0}{c\frac{r}{r_{\rm v}}(1 + c\frac{r}{r_{\rm v}})^2}$$

with circular velocity

$$V_{\rm c}^2(r) = \frac{{V_{\rm v}}^2 g(c) r_{\rm v}}{r}\left[\ln\left(1 + c\,\frac{r}{r_{\rm v}}\right) - \frac{c\,\frac{r}{r_{\rm v}}}{1 + c\,\frac{r}{r_{\rm v}}}\right]$$

where $\delta_{\rm c}$ is the density contrast at the virial radius, c the concentration, $r_{\rm v}$ the virial radius, and $v_{\rm v}$ the circular velocity at the virial radius. We use the concentration and the virial radius as free parameters for the dark matter halo. Figure 14 (bottom left) shows the fit in the maximum disk hypothesis ($M/L = 3.6$, $r_{\rm v} = 316 \pm 23$ kpc, $c = 6.3 \pm 0.8$). This gives a virial mass of $M_{\rm vir} = 1.5 \times 10^{12}$ $M_\odot$ and a disk and dark matter mass within the last measured point, which are very similar to the combination of a maximum disk and an isothermal halo. The value of the concentration, however, appears very low compared to the one predicted by CDM simulations (e.g. Wechsler et al. 2002). If we keep the M/L free in the fit, we obtain $M/L = 3.5$, very close to the maximum disk hypothesis.

When trying to minimize the disk contribution in the fit, the values of the concentration tend to increase considerably. Since the typical values for a DM halo of galactic mass range from 10 to 20, we set an upper limit of 20 to the concentration. In this way a minimum disk fit corresponds to a maximum concentration fit. Figure 14 (bottom right) shows the result of the maximum concentration fit ($c = 20$, $M/L = 2.8 \pm 0.1$, $r_{\rm v} = 219 \pm 4$ kpc). The quality of the fit is not as good as in the maximum disk. In particular, the feature at 2 kpc radius is not reproduced and in the outer region a discrepancy with the observed velocities begins to show up. For a further discussion see Sect. 8.

7. Halo gas

Recent H I observations of edge-on spiral galaxies (Swaters et al. 1997; Matthews & Wood 2003) have revealed the presence of extra-planar gas located at several kpc above and below the galaxy plane and with a rotational velocity that is lower

[1] We assumed $M_{\odot,B} = 5.48$ and $M_{\odot,F} = 4.5$.

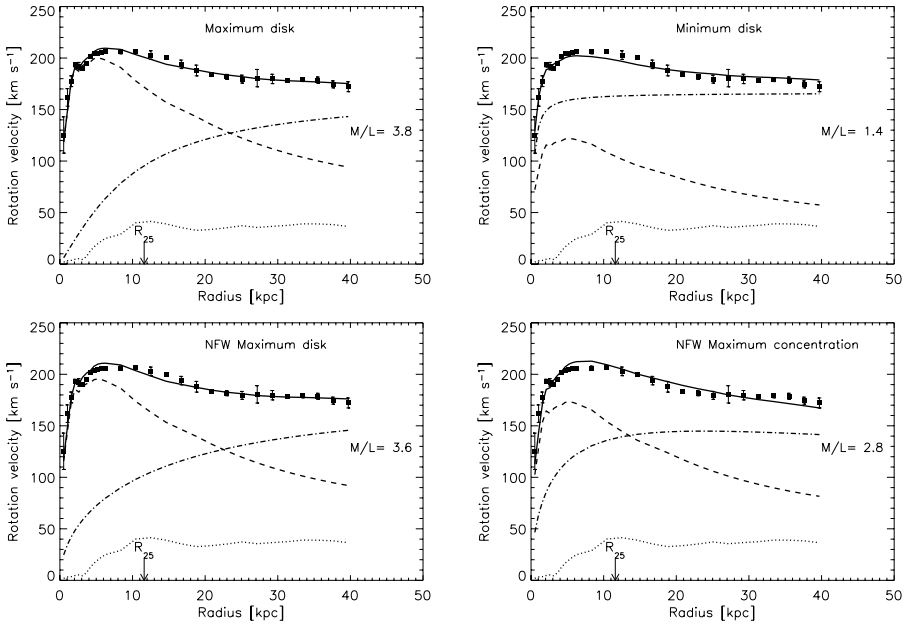

Fig. 14. Mass models for NGC 5055. The contributions of the different mass components to the observed circular velocities are shown: gas (dotted line), stars (dashed line), and DM halo (dash-dot line). The full thick line shows the total contribution to the rotation velocity.

than the gas in the disk. Such peculiar kinematics made it possible to also detect such a halo H I in less inclined systems (e.g. NGC 2403, Fraternali et al. 2002), where it shows up in *p-v* diagrams along the major axis as a wing at low rotational velocities.

We investigated the presence of such gas in NGC 5055 by analyzing both the channel maps and the position-velocity diagrams. Figure 4 (left) shows a p-v diagram at a resolution of 28″ along the major axis. In the inner parts of this diagram, the line profiles are not symmetric but have "wings" extending towards the systemic velocity (low rotational velocity). In the receding side the "lagging" gas is mostly visible within about 7 kpc from the centre and shows a maximum projected difference of about 100 km s^{-1} from the rotational velocity. In the approaching side, there is a hint of very high velocity gas up to ∼200 km s^{-1} of a projected difference from rotation. In both cases the emission comes from regions inside the bright optical disk. Our observations, with an integration time of 24 h, were not deep enough to allow a complete analysis of the halo gas. So we did not perform any separation of this gas from the "cold" thin disk.

8. Discussion

The distribution and dynamics of the neutral gas in the nearby spiral galaxy NGC 5055 were studied using new high-sensitivity WSRT observations. In this section we discuss the main results.

8.1. H I density distribution and warp

The H I disk of NGC 5055 extends out to 19′ (40 kpc) from the centre, far beyond the optical radius (R_{25} = 5′.5). The outer parts of the H I disk are strongly warped as indicated by the total H I map and the velocity field in Fig. 1. In the tilted ring model for the disk, the outer rings are warped by about 20° with respect to the inner ones (θ angle in Fig. 9, panel 3 from the top). The warp begins at about 5′ (10 kpc) at the end of the bright optical disk. This behaviour is commonly observed in spiral galaxies (Briggs 1990; Garcia-Ruiz et al. 2002). This is also close to the edge of the bright H I disk where the H I surface density drops from 5.5 to about 1 $M_\odot$ pc^{-2} (Fig. 13). Further out, the density is below 1 $M_\odot$ pc^{-2} and continues to decrease slowly by about 0.06 $M_\odot$ pc^{-2} kpc^{-1}. The density distribution of H I in the region of the warp is not homogeneous, and spiral-like features are clearly visible in the high resolution total H I map (Fig. 1, top-right panel).

Despite the mild asymmetries between the approaching and the receding sides described in Sect. 5, the warp of NGC 5055 is highly symmetric both in geometry (see Figs. 6 and 9) and in kinematics, as is clearly shown by the velocity field (Fig. 1, lower right panel). Such a symmetry is remarkable if one considers the exceptional extent of the warp itself. The orbital time (roughly a lower limit to the life time of the warp) at R = 40 kpc is about 1.5 Gyr. This suggests that the warp of NGC 5055 is a long-lived phenomenon.

Galactic warps have been known to exist for several decades, but a satisfactory dynamical explanation has not been found yet. The dark matter halo may play an important role, as suggested by the empirical rule that warps start at the end of the stellar disks where the dark matter potential becomes dynamically dominant (Briggs 1990). Several mechanisms have been proposed for the formation (and/or maintenance) of warps, such as accretion of intergalactic material with different angular momentum (Jiang & Binney 1999), interactions with companion galaxies (Hunter & Toomre 1969), or misalignment between the disk and the dark halo (Debattista & Sellwood 1999).

In NGC 5055, the warp tends to align the position angle of the outer disk towards the companion galaxy UGC 8313

(see Fig. 1). This may suggest a role of the latter in the formation and/or maintenance of the warp. However, the motion of UGC 8313 is retrograde with respect to that of the disk. This implies that the dynamical effect of UGC 8313 is likely to be small. Moreover, given the large difference in mass, one can expect that NGC 5055 would have a greater influence on UGC 8313, which appears undisturbed. Therefore, the interaction between the two galaxies cannot be strong.

8.2. The dynamics

The rotation curve of NGC 5055 (Fig. 10) rises steeply in the inner parts, reaching the maximum (206 km s^{-1}) at 4 kpc (2′) from the centre. Between 10 and 20 kpc, it shows a decline of about 25 km s^{-1}, and beyond 20 kpc, it remains almost flat out to the last measured point (at 40 kpc). Two features of this rotation curve deserve particular attention: one is the inner bump at about 2 kpc from the centre and the other is the decline at 10−20 kpc.

The inner bump is observed in both the approaching and the receding sides (Fig. 10). The excess velocity in the bump is of the order of 10 km s^{-1}. There is no doubt that the bump is real (cf. Fig. 4), because it occurs in a region where both inclination and position angles are almost constant (Figs. 5, 6, 9) and is present in both halves of the disk (Figs. 7 and 10). Similar features are often observed in the inner regions of spiral galaxies (Sancisi 2004). A comparison with the photometric profile of NGC 5055 (Fig. 12) shows that there is a corresponding bump in surface brightness within 2 kpc of the centre. Indeed, the maximum disk fit to the rotation curve reproduces the inner shape of the rotation curve (Fig. 14, left panels) rather accurately, whereas fits with dominant smooth halo components do not (Fig. 14, right panels). This strongly suggests that, in the inner part of the galaxy, the dominant component is the stellar one or is a dark component distributed like the stars. In other words, the stars trace the gravitational potential in the inner parts.

As to the decline beyond 10 kpc, is it real or could it be the result of an imperfect model fitting of the warped disk? It is clear that correct determination of the two parameters (inclination and position angles) that describes the projected geometry of the warp is crucial for deriving correct values for the rotation velocity. Let us first consider the position angle. The kinematical major axis of a rotating disk is the location where the projected rotation velocities reach their highest values. When the position angle varies with R, the major axis is not a straight line but is "S" shaped if the warp is symmetric. In Fig. 4 (right), the shape of the actual major axis of NGC 5055 is plotted over a velocity field at 28″ resolution. In the left panel of Fig. 4, the p-v plot along the "S" shaped major axis is shown with the projected rotation curve of the galaxy overlaid (white squares). The squares follow the peaks of the line profiles very closely, and the small discrepancies are mainly due to asymmetries between the approaching and the receding sides. Thus the fitted position angles for each ring do represent the location of the maxima in the velocity field.

Clearly, the decline in the rotation curve is not caused by an error in the determination of the position angle. Now consider the inclination angle. An error in determining the inclination angles of the outer rings would affect the derived rotation velocities. The decline of the outer rotation curve would indeed disappear if the values of the inclination angles were wrong by about 10° (more face-on) beyond 10 kpc. Such a high systematic error is unlikely considering the small errors in the fit and the very small differences between the approaching and receding sides (Figs. 6, 9). Moreover, a fit of the outer contours (at $R \simeq 18'$) of the total H I map gives a value for the outer inclination of 57.6°, very close to the one obtained at the same radius with the tilted ring fit (Figs. 6, 9). In conclusion, the declining rotation curve must be a real feature of the dynamics of NGC 5055.

Such a decrease in the outer parts of the rotation curve has been observed in other galaxies (Casertano & van Gorkom 1991; Bottema & Verheijen 2002). Interestingly, this decline happens to be just outside the bright optical disk ($R_{25} = 5.5'$) where the warp starts (Fig. 9) and the H I surface density drops abruptly (Fig. 13). This suggests that such a decline may be related to the "end" of the bright stellar disk where the dark matter halo starts to dominate. The decompositions of the rotation curve (Fig. 14) show that such a decline can be reproduced by a large set of parameters: different M/L values and different density profiles of the dark matter halo. However for an isothermal dark halo there seems to be a lower limit for the M/L ratio of the stellar disk. The top right panel of Fig. 14 shows the fit for a $M/L = 1.4$, which we consider as the minimum disk fit. Such a fit shows discrepancies between the data and the model that are larger than in the maximum disk fit. For lower M/L ratios than this value, the fit is unacceptable. The minimum disk fit obtained is very close to a so-called Bottema disk, where 66% of the observed maximum rotational velocity is contributed by the luminous matter (Bottema 1997). Figure 14 (lower panels) also shows the fits obtained with a universal profile for the dark matter halo (Navarro et al. 1995). The parameter space permitted by this fit is even smaller, going from a maximum disk ($M/L = 3.6$) to a minimum disk with $M/L = 2.8$. Note, however, that the inner rotation curve is better reproduced with a maximum disk fit.

In conclusion, the maximum disk fit (with either isothermal or NFW profile for the dark component) can satisfactorily reproduce the main features of the rotation curve of NGC 5055 (inner bump and outer decline). This gives a natural explanation for the decline of the rotation curve in terms of a transition from the region where the stellar disk is dynamically dominant and the outer parts where the dark halo starts to dominate. The existence of two such different dynamical regimes for the inner and the outer parts of the galaxy may be related to the outer warping of the disk (Sect. 8.1).

8.3. The lopsidedness: a disk/DM halo offset?

We have described the mild asymmetries in both the warp and the kinematics of NGC 5055 and investigated the tilted ring models and, in particular, the consequences of a change in the

systemic velocity and in the position of the centre from the inner to the outer rings of the disk. We showed that such a change leads to symmetrical rotation curves on the two halves of the disk and also to a striking symmetry for the position and the inclination angles on the two sides (compare Figs. 6 and 9). Although it may not be surprising that by allowing the systemic velocity to vary in each ring, symmetric rotation curves are obtained, it is remarkable that also the position and inclination angles are made symmetrical here (and consequently also the other angles that describe the warp). Indeed, a simple variation with radius of centre and systemic velocity in the tilted ring fit has led to a complete symmetrization of the system, both kinematically and geometrically. It appears that we are dealing here with fundamental aspects of the dynamics of NGC 5055 and that there is probably a relation with the potential and with the two regimes – a stellar disk dominating in the inner and a dark halo in the outer parts – discussed in the previous sections. The following facts also support this view:

1. The systemic velocity does not vary randomly. On the contrary, it stays roughly constant in the inner region (within 8 kpc) and, at the end of the bright optical disk, rises and remains approximately constant around a higher value.
2. The position of the centre of the galaxy obtained with the two assumed systemic velocities also varies (by about 1.8 kpc) from the inner to the outer rings, and towards the western side where the H I disk of NGC 5055 is more extended. The displaced outer rings resulting from this shift of the centre roughly match the asymmetry in the H I density distribution.
3. The changes in systemic velocity and position of the centre not only produce symmetric rotation curves but also symmetrize the position and inclination angles and hence affect the entire kinematics and geometry of the galaxy.
4. The displacement and the change in systemic velocity of the outer rings are towards the projected position and the systemic velocity of the companion UGC 8313. But it is unclear whether this points to a dynamical influence of the companion on the outer parts of NGC 5055 as already discussed in relation to the warp (Sect. 8.1).

In our analysis of NGC 5055, we relaxed two of the basic assumptions – the spatial and the kinematical centre of the system do not vary with radius – that are usually made in the tilted ring modeling of a galaxy. The results are a strong indication that this is a very powerful way to parameterize the asymmetries of the system. But in this approach the orbits of the gas are still circular, and the velocity is constant over the whole orbit. If the shifting of the centre with radius is related to a shifting of the mass centroid, one expects the orbits of the particles to be elliptical. If the perturbation of the circular orbit is small (i.e. the potential has a small stationary perturbation), an analytical description of the motion can be given via the theory of epicycles.

In order to test our results, we performed a decomposition of the velocity field of NGC 5055 into harmonic components following the approach of Schoenmakers et al. (1997) and found that the dominant harmonic terms are $m = 0$ and $m = 2$ (in the outer parts). This confirms our previous findings: the $m = 0$ term can indeed be seen as a change in systemic velocity, whilst the $m = 2$ term is related to a shift of the centre of the galaxy (see Schoenmakers et al. 1997). In particular, in NGC 5055 the s_2 term is significantly different from 0 beyond 14 kpc, and this is, in fact, the radius where the position of the centre shifts significantly from the inner value (Fig. 8).

As pointed out by Schoenmakers et al. (1997), the presence of an m-term stationary perturbation of the potential produces $m-1$ and $m+1$ terms in the residual velocity field. These terms are mixed, and their reciprocal amplitudes depend mainly on the viewing angle of the perturbation (see also Swaters et al. 1999). Our harmonic analysis suggests the presence of an $m = 1$ term perturbation of the potential in NGC 5055.

In short, we have shown a new approach to parameterizing the kinematical and morphological asymmetries in the spiral galaxy NGC 5055 that gives the same results as the harmonic analysis of the velocity field. In this approach the lopsidedness is related to a transition from the inner parts where the dynamically dominant component is the (axi-symmetric) stellar disk to the outer parts which are dominated by a displaced (or lopsided) dark matter halo. This interpretation is supported in NGC 5055 by the beginning of the warp and the decline of the rotation curve at the transition radius. Finally, we note that in our approach the kinematical and the morphological lopsidedness both tend to disappear as the centres of the outer rings shift in the direction where the H I distribution is more extended. It is not clear whether the presence of the companion galaxy may also play a role.

9. Summary

We carried out a detailed 21-cm line study of the spiral galaxy NGC 5055 using new H I observations recently obtained with the WSRT. New interesting aspects have emerged concerning the morphology and the dynamics of this galaxy:

1. NGC 5055 has a very extended ($R \sim 40$ kpc) and warped H I disk. The warp is highly symmetric, and its long revolution time (1.5 Gyr) indicates that it is a long-lived phenomenon. The warp begins at the end of the bright stellar disk and is oriented in the direction of the companion galaxy UGC 8313.
2. The rotation curve of NGC 5055 shows two main features: a bump at about 2 kpc from the centre, which clearly corresponds to a bump in the optical surface brightness, and a velocity decline of about 25 km s^{-1} at the end of the bright optical disk. The standard analysis of the rotation curve into luminous and dark matter components shows that only "maximum disk" fits are able to reproduce both features at the same time. Furthermore, for an acceptable fitting of the rotation curve in its declining outer parts, the stellar disk must be rather massive. In the solution with a quasi-isothermal dark matter halo a firm lower limit has been set to the disk mass-to-light ratio ($M/L \gtrsim 1.4$).
3. Mild asymmetries between the approaching and receding sides of NGC 5055 are present both in the kinematics and in the morphology. The tilted ring analysis of the velocity field shows that if the systemic velocity and the position of

the centre are allowed to vary with radius from the inner to the outer parts, the asymmetries are explained and a striking geometrical and kinematical symmetrization of the system is achieved.

All these results suggest that NGC 5055 has two dynamical regimes: an inner one dominated by the luminous matter and an outer one, dominated by a dark matter halo offset with respect to the inner disk. The transition radius (about 10 kpc) is the region where:

- the warp begins;
- the stellar and the H I disk begin to fade out;
- the rotation curve starts to decline;
- the systemic velocity changes.

It is not clear whether the companion galaxy UGC 8313 has any significant role in causing the observed asymmetry.

Acknowledgements. We thank Thijs van der Hulst for insightful comments and improvements to the manuscript. G.B. is grateful to the Kapteyn Astronomical Institute for their hospitality and financial support in the early stages of this work. The WSRT is operated by the Netherlands Foundation for Research in Astronomy (ASTRON) with the support from the Netherlands Foundation for Scientific Research (NWO). This research made use of the NASA Extragalactic Database (NED). The Digitized Sky Survey was produced at the Space Telescope Science Institute under US Government grant NAG W-2166.

References

Begeman, K. G. 1987, Ph.D. Thesis, University of Groningen, NL
Boomsma, R., Oosterloo, T. A., Fraternali, F., van der Hulst, J. M., & Sancisi, R. 2005, A&A, 431, 65
Bosma, A. 1978, Ph.D. Thesis, University of Groningen, NL
Bottema, R. 1993, A&A, 275, 16
Bottema, R. 1997, A&A, 328, 517
Bottema, R., & Verheijen, M. A. W. 2002, A&A, 388, 793
Briggs, F. H. 1990, AJ, 352, 15
Broeils, A. H. 1992, Ph.D. Thesis, University of Groningen, NL
Burke, B. F. 1957, AJ, 62, 90
Casertano, S. 1983, MNRAS, 203, 735
Casertano, S., & van Gorkom, J. H. 1991, AJ, 101, 1231
Clark, B. G. 1980, A&A, 89, 377
Debattista, V. P., & Sellwood, J. A. 1999, ApJ, 513, L107
Fraternali, F., van Moorsel, G., Sancisi, R., & Oosterloo, T. 2002, AJ, 123, 3124
Fraternali, F., Oosterloo, T., Sancisi, R., & Swaters, R. 2005, in Extra-planar Gas, ed. R. Braun, ASP Conf. Proc., 331, 239
Garcia-Ruiz, I., Sancisi, R., & Kuijken, K. 2002, A&A, 394, 769
Holmberg, E. 1958, Medd. Lund Obs. Ser. II, No. 136
Hunter, C., & Toomre, A. 1969, ApJ, 155, 747
Jiang, I. G., & Binney, J. 1999, MNRAS, 303, L7
Kamphuis, J. 1993, Ph.D. Thesis, University of Groningen, NL
Kamphuis, J., & Briggs, F. 1992, A&A, 253, 335
Kahn, F. D., & Woltjer, L. 1959, ApJ, 130, 705
Kent, S. M. 1987, AJ, 93, 816
Kerr, F. J. 1957, AJ, 62, 93
Maoz, D., Filippenko, A. V., Ho, L. C., et al. 1996, ApJ, 107, 215
Matthews, L. D., & Wood, K. 2003, ApJ, 593, 721
Navarro, J. F., Frenk, C. S., & White, S. D. 1995, MNRAS, 275, 720
Navarro, J. F., Frenk, C. S., & White, S. D. 1996, ApJ, 462, 563
Persic, M., & Salucci, P. 1991, ApJ, 368, 60
Pierce, M. 1994, ApJ, 430, 53
Rots, A. H. 1980, A&A, 41, 189
Sancisi, R. 2004, in Dark Matter in Galaxies, ed. S. D. Ryder, D. J. Pisano, M. A. Walker, & K. C. Freeman (San Francisco: PASP), IAU Symp., 220, 233
Sault, R. J., Teuben, P. J., & Wright, M. C. H. 1995, in Astronomical Data Analysis Software and Systems IV, ed. R. A. Shaw, H. E. Payne, & J. J. E. Hayes (San Francisco: ASP), ASP Conf. Ser., 77, 433
Schoenmakers, R. H. M., Franx, M., & de Zeeuw, P. T. 1997, MNRAS, 292, 349
Schwarz, U. J. 1985, A&A, 142, 273
Sparke, L. S., & Casertano, S. 1988, MNRAS, 234, 873
Swaters, R. A., Sancisi, R., & van der Hulst, J. M. 1997, ApJ, 491, 140
Swaters, R. A., Schoenmakers, R. H. M., Sancisi, R., & van Albada, T. S. 1999, MNRAS, 304, 330
Tully, R. B. 1988, Science, 242, 310
van der Hulst, J. M., Terlouw, J. P., Begeman, K., Zwitser, W., & Roelfsema, P. R. 1992, in Astronomical Data Analysis Software and Systems I, ed. D. M. Worall, C. Biemesderfer, & J. Barnes (San Francisco: ASP), ASP Conf. Ser., 25, 131
de Vaucouleurs, G., et al. 1976, Second Reference Catalogue of Bright Galaxies (Austin: University of Texas Press)
Wechsler, R. H., Bullock, J. S., Primack, J. R., Kravtsov, A. V., & Avishai, D. A. 2002, ApJ, 568, 52
Wevers, B. M. H. R. 1984, Ph.D. Thesis, University of Groningen, NL